UC Berkeley

UC Berkeley Previously Published Works

Title

Two-dimensional electronic–vibrational spectroscopy: Exploring the interplay of electrons and nuclei in excited state molecular dynamics

Permalink

https://escholarship.org/uc/item/76c069sp

Journal

The Journal of Chemical Physics, 155(2)

ISSN

0021-9606

Authors

Arsenault, Eric A
Bhattacharyya, Pallavi
Yoneda, Yusuke
et al.

Publication Date

2021-07-14

DOI

10.1063/5.0053042

Peer reviewed

eScholarship.org Powered by the California Digital Library
University of California

The Journal of Chemical Physics

Two-dimensional electronic–vibrational spectroscopy: Exploring the interplay of electrons and nuclei in excited state molecular dynamics

Cite as: J. Chem. Phys. **155**, 020901 (2021); https://doi.org/10.1063/5.0053042
Submitted: 03 April 2021 • Accepted: 09 May 2021 • Published Online: 08 July 2021

Eric A. Arsenault, Pallavi Bhattacharyya, Yusuke Yoneda, et al.

COLLECTIONS

Paper published as part of the special topic on Coherent Multidimensional Spectroscopy

This paper was selected as Featured

View Online Export Citation CrossMark

ARTICLES YOU MAY BE INTERESTED IN

Chemical physics software
The Journal of Chemical Physics **155**, 010401 (2021); https://doi.org/10.1063/5.0059886

Nuclear–electronic orbital methods: Foundations and prospects
The Journal of Chemical Physics **155**, 030901 (2021); https://doi.org/10.1063/5.0053576

Multidimensional electronic spectroscopy in high-definition–Combining spectral, temporal, and spatial resolutions
The Journal of Chemical Physics **154**, 230901 (2021); https://doi.org/10.1063/5.0052234

Challenge us.
What are your needs for periodic signal detection?
Watch

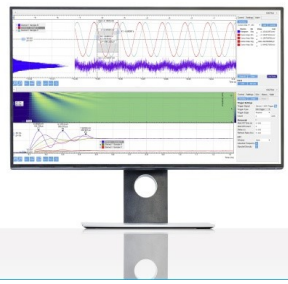

Zurich Instruments

© 2021 Author(s).

The Journal of Chemical Physics PERSPECTIVE scitation.org/journal/jcp

Two-dimensional electronic–vibrational spectroscopy: Exploring the interplay of electrons and nuclei in excited state molecular dynamics

Cite as: J. Chem. Phys. 155, 020901 (2021); doi: 10.1063/5.0053042
Submitted: 3 April 2021 • Accepted: 9 May 2021 •
Published Online: 8 July 2021

View Online Export Citation CrossMark

Eric A. Arsenault,[1,2,3] Pallavi Bhattacharyya,[1,2,3] Yusuke Yoneda,[1,3,a)] and Graham R. Fleming[1,2,3,b)]

AFFILIATIONS

[1] Department of Chemistry, University of California, Berkeley, California 94720, USA
[2] Kavli Energy Nanoscience Institute at Berkeley, Berkeley, California 94720, USA
[3] Molecular Biophysics and Integrated Bioimaging Division, Lawrence Berkeley National Laboratory, Berkeley, California 94720, USA

Note: This paper is part of the JCP Special Topic on Coherent Multidimensional Spectroscopy.
[a)] **Present Address:** Research Center of Integrative Molecular Systems, Institute for Molecular Science, National Institute of Natural Sciences, Okazaki, Aichi 444-8585, Japan.
[b)] **Author to whom correspondence should be addressed:** grfleming@lbl.gov

ABSTRACT

Two-dimensional electronic–vibrational spectroscopy (2DEVS) is an emerging spectroscopic technique which exploits two different frequency ranges for the excitation (visible) and detection (infrared) axes of a 2D spectrum. In contrast to degenerate 2D techniques, such as 2D electronic or 2D infrared spectroscopy, the spectral features of a 2DEV spectrum report cross correlations between fluctuating electronic and vibrational energy gaps rather than autocorrelations as in the degenerate spectroscopies. The center line slope of the spectral features reports on this cross correlation function directly and can reveal specific electronic–vibrational couplings and rapid changes in the electronic structure, for example. The involvement of the two types of transition moments, visible and infrared, makes 2DEVS very sensitive to electronic and vibronic mixing. 2DEV spectra also feature improved spectral resolution, making the method valuable for unraveling the highly congested spectra of molecular complexes. The unique features of 2DEVS are illustrated in this paper with specific examples and their origin described at an intuitive level with references to formal derivations provided. Although early in its development and far from fully explored, 2DEVS has already proven to be a valuable addition to the tool box of ultrafast nonlinear optical spectroscopy and is of promising potential in future efforts to explore the intricate connection between electronic and vibrational nuclear degrees of freedom in energy and charge transport applications.

© 2021 Author(s). All article content, except where otherwise noted, is licensed under a Creative Commons Attribution (CC BY) license (http://creativecommons.org/licenses/by/4.0/). https://doi.org/10.1063/5.0053042

I. INTRODUCTION

The method of two-dimensional electronic–vibrational spectroscopy (2DEVS), introduced in 2014 by Oliver *et al.*,[1] was proposed as a technique for correlating the evolution of the nuclear degrees of freedom (DoF) with that of the electronic DoF in optically excited molecules and complexes. For example, a progressive shift in an excited state vibrational frequency as solvation proceeds reports on the changing electronic structure as the solvent rearranges.[1] It was quickly realized that the domain of applicability of 2DEVS was much broader than simple non-reactive systems. Initially, in energy transfer (ET) systems, vibrations were viewed as reporters or flags for the location of excitations in a pigment–protein complex, for example.[2] However, it soon became clear that oscillatory structures in 2DEV spectra of molecular complexes could reveal the role of vibronic interactions in facilitating energy flow.[3] A parallel investigation of vibronic effects in ultrafast charge transfer (CT) via 2DEVS was pioneered by Gaynor *et al.*[4]

A comparison of 2DEVS with the degenerate third-order 2D infrared[5–8] and 2D electronic[9–11] spectroscopies (2DIRS and 2DES,

© Author(s) 2021

respectively) can aid in clarifying the strengths and weaknesses of each method. 2DIRS and 2DES have been extensively analyzed and modeled,[12–14] and our aim here is to bring out some of the apparently unique characteristics of 2DEV spectra through comparison. A related technique in which the vibrational excitation precedes the electronic excitation, 2DVES, was developed by Courtney *et al.*[15] In this Perspective, we focus on 2DEVS.

An immediate difference is that while the degenerate spectroscopies measure quantities related to autocorrelation functions of transition frequency fluctuations or cross correlations between transitions arising from the same types of DoF, 2DEV spectra contain cross correlations of the fluctuating electronic and vibrational energy gaps, i.e., disparate DoF. These cross correlation functions can be characterized by the evolution of the center line slope (CLS) of the spectral features.[16,17] Because 2DEV features involve different types of transition moments, electronic and vibrational, the spectra can be very sensitive to electronic and vibronic mixing through substantial alteration to the IR transition moments. This is distinct from degenerate spectroscopies where features depend only on one type of transition moment. The result is that weak transitions not readily apparent in 1D or 2D electronic spectra can become prominent in 2DEV spectra.

Degenerate spectroscopies also contain a diagonal along which is displayed the absorption spectrum and, in 2DIR spectra, includes the anharmonic splitting. 2DEV spectra, on the other hand, are intrinsically off-diagonal. Here, the detection of vibrational features spreads out the electronic excitation along the detection axis, often giving remarkably improved resolution in the electronic spectrum. The comparison of diagonal and off-diagonal features and of diagonal and anti-diagonal widths has long been of value in 2DES and 2DIRS, as has the comparison of rephasing and non-rephasing spectra.[12–14] 2DEV spectra, being entirely off-diagonal and exhibiting rather little rephasing, do not allow such comparisons.[18]

Recording spectra as a function of waiting time in 2DES or 2DIRS generally results in spectra that have an intuitive appearance, such as the growth of off-diagonal features resulting from energy transport in exciton systems, for example. In 2DEV spectra, however, the evolution of the spectra with waiting time is not always intuitive. This is clearly apparent in the same example as just given, where the entire 2DEV spectrum becomes increasingly symmetric around the excitation axis as ET proceeds. In 2DIR spectra of chemical exchange systems, the spectra do become symmetric, as a result of the reversibility of the exchange process,[12] but only unidirectional transfer is required in 2DEV spectra.

All 2D spectroscopies gain spectral resolution by spreading out the peaks into a second dimension. The good spectral resolution in 2DEV spectra along the detection (IR) axis is not surprising, but in many 2DEV spectra, enhanced resolution along the excitation (visible) axis as compared to linear absorption or 2D electronic spectra is also noticeable. This has enabled the clear identification of the involvement of specific vibrational modes in relaxation over particular energy gaps in an excitonic manifold,[3] for example, or of vibronic coupling across specific metal-to-ligand charge transfer (MLCT) states.[4] This improved resolution along the excitation axis also enables tracking the temporal evolution of the excitation frequency distribution at specific vibrational frequencies that can be related back to individual components or electronic states in heavily overlapped spectral regions of multi-component systems.[19]

Of course, there are multiple aspects of similarity in these three 2D spectroscopies, such as the exploitation of photon polarization to enhance information content, and clearly, the three methods should be regarded as complementary with the choice of the method dictated by the questions asked.

II. ORIGIN OF THE 2DEVS SIGNAL

2DEVS is a four-wave mixing process where the interactions of the three pulses (in this case, two visible and one IR) with the sample produce the third-order nonlinear signal (pulse sequence shown in Fig. 1). This signal can be understood as arising from the third-order polarization, which, within a perturbative framework, is given by the convolution of the third-order response function, $S^{(3)}(t_1,t_2,t_3)$, with the electric field of the incident pulses, $E(t)$,[20]

$$P^{(3)}(t_1,t_2,t_3) = \int_0^\infty \int_0^\infty \int_0^\infty S^{(3)}(t_1,t_2,t_3)E(t-t_3-t_2-t_1) \times E(t-t_3-t_2)E(t-t_3)dt_1dt_2dt_3. \quad (1)$$

Considering that the electric field of the pulse sequence is given by

$$E(t) = \sum_{j=1}^{3} A_j(t-t_j)e^{-i\omega_j(t-t_j)+i\boldsymbol{k}_j\cdot\boldsymbol{r}+i\phi_j} + c.c., \quad (2)$$

where A_j, ω_j, $\boldsymbol{k}_j$, and ϕ_j are the temporal envelope, carrier frequency, wavevector, and phase of the jth pulse, respectively, the third-order polarization is a complicated quantity as a result of the many contributing signal pathways.

Typically, degenerate or near-degenerate 2D spectroscopies utilize phase matching conditions to spatially separate the desired signal pathways from the others inherently generated through the light–matter interactions. In practice, these conditions are enforced through the physical geometry (e.g., boxcar geometry) of the incident beams.[9] However, what distinguishes 2DEVS in this regard is that there is approximately an order of magnitude difference between the wavelengths of the highly nondegenerate visible excitation pulses and the IR detection pulse. This severely limits the practical experimental geometries by which this type of spectroscopy can be performed in order to obtain a background-free signal.[21] Rather, the implementation of phase cycling with a pump–probe geometry

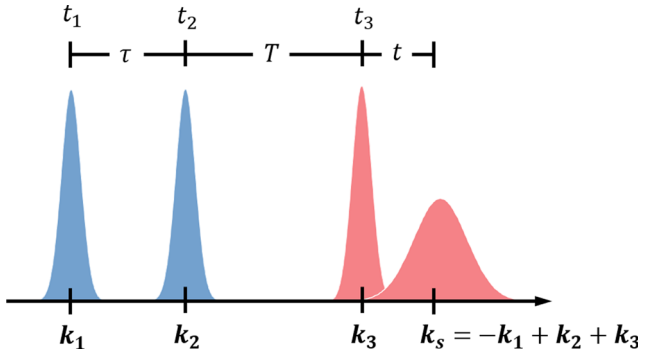

FIG. 1. 2DEVS pulse sequence. The blue pulses, k_1 and k_2, indicate electronically resonant excitation interactions, and the red pulse, k_3, indicates a vibrationally resonant detection interaction. Finally, k_s represents the emitted signal following the three previous light–matter interactions occurring at t_1, t_2, and t_3. The relative delays between fields are denoted as τ, T (termed the waiting time), and t.

© Author(s) 2021

($\boldsymbol{k}_1 = \boldsymbol{k}_2 \neq \boldsymbol{k}_3$) is the most useful means for isolating the 2DEV signal. In the pump–probe geometry, the third-order signal intensity is given by

$$I^{(3)}(t_1,t_2,\omega_3) \propto \left|E_3(\omega_3)\left(1+\tilde{S}^{(3)}_{113}(t_1,t_2,\omega_3) + \tilde{S}^{(3)}_{223}(t_1,t_2,\omega_3)+\tilde{S}^{(3)}_{123}(t_1,t_2,\omega_3)\right)\right|^2, \quad (3)$$

where $E_3(\omega_3)$ is the IR probe field, which also serves as the local oscillator, $\tilde{S}^{(3)}_{113}(t_1,t_2,\omega_3)$ and $\tilde{S}^{(3)}_{223}(t_1,t_2,\omega_3)$ are the pump–probe background signals, and $\tilde{S}^{(3)}_{123}(t_1,t_2,\omega_3)$ is the 2DEV signal. Here,

$$S^{(3)}_{jk3}(t_1,t_2,\omega_3)E_3(\omega_3) = \int_0^\infty\int_0^\infty\int_0^\infty e^{-i\omega_3 t_3}S^{(3)}(t_1,t_2,t_3) \times E_j(t-t_3-t_2-t_1)E_k(t-t_3-t_2) \times E_3(t-t_3)dt_1dt_2dt_3 \quad (4)$$

is the Fourier transform over t_3 of the convolution of the third-order response function with the electric fields of the pulses. The intensity can be rewritten as

$$I^{(3)}(t_1,t_2,\omega_3;\Delta\phi_{12}) \propto \left|\left(1+\tilde{S}^{(3)}_{113}(t_1,t_2,\omega_3)+\tilde{S}^{(3)}_{223}(t_1,t_2,\omega_3)\right) \times E_3(\omega_3)\right|^2 + \left|\left(\tilde{S}^{(3)}_{123}(t_1,t_2,\omega_3)\right)E_3(\omega_3)\right|^2 + 2\mathrm{Re}\left[e^{i\Delta\phi_{12}}\tilde{S}^{(3)}_{123}(t_1,t_2,\omega_3)\left(1+\tilde{S}^{(3)}_{113}(t_1,t_2,\omega_3) + \tilde{S}^{(3)}_{223}(t_1,t_2,\omega_3)\right]^*\right)|E_3(\omega_3)|^2, \quad (5)$$

where the dependence of $\tilde{S}^{(3)}_{123}(t_1,t_2,\omega_3)$ on the interpulse phase difference between the two pump pulses has been shown explicitly—the 2DEV signal acquires an overall phase prefactor, while the largest undesirable signals do not. In this way, the 2DEV signal can be effectively isolated by repeating the measurement n times with values of $\Delta\phi_{12}$ stepped by $\frac{2\pi}{n}$ and summing the following results:[22,23]

$$\begin{aligned}&\frac{1}{n}\sum_{j=1}^{n-1}e^{-i(2\pi j/n)}\left|E_3(\omega_3)\left(1+\tilde{S}^{(3)}_{113}(t_1,t_2,\omega_3)+\tilde{S}^{(3)}_{223}(t_1,t_2,\omega_3)+\tilde{S}^{(3)}_{123}(t_1,t_2,\omega_3)\right)\right|^2\\ &= 2\tilde{S}^{(3)}_{123}(t_1,t_2,\omega_3)\mathrm{Re}\left[\left(1+\tilde{S}^{(3)}_{113}(t_1,t_2,\omega_3)+\tilde{S}^{(3)}_{223}(t_1,t_2,\omega_3)\right)^*\right]|E_3(\omega_3)|^2\\ &\simeq 2\tilde{S}^{(3)}_{123}(t_1,t_2,\omega_3)|E_3(\omega_3)|^2. \end{aligned} \quad (6)$$

While the cross terms between the pump–probe and 2DEV signals cannot be completely suppressed, these terms scale quadratically with the third-order field and thus are negligible compared to the desired signal, which scales linearly with the third-order field. The isolation of the 2DEV signal is completed following division by a reference field (identical to the probe field). Finally, to obtain the absorptive 2DEV spectrum, a Fourier transform along t_1 of the signal is performed. Often, however, further processing is done in order to achieve a higher quality spectrum.

III. EXPERIMENTAL IMPLEMENTATION OF 2DEVS

The 2DEV spectrometer in our lab, for the reasons described above, is based on a pump–probe design. In practice, it is equivalent to that of a visible pump-IR probe spectrometer fitted with a pulse shaper in the optical path of the visible pump in order to (1) generate and (2) control the relative phase and temporal delay between the visible pump pulse pair. A schematic of the experimental design is shown in Fig. 2. The driving laser consists of a Ti:Sapphire (Ti:Saph) regenerative amplifier (Legend Elite, Coherent) seeded by a Ti:Saph oscillator (Vitara-S, Coherent), which pumps both a non-collinear optical parametric amplifier (NOPA) and an optical parametric amplifier (OPA)-pumped difference frequency generation (DFG) source to generate the visible excitation and mid-IR detection pulses, respectively.

For the reasons described in Sec. II, the output of the NOPA, following pre-dispersion compensation in a prism pair, is directed into a pulse shaper (Dazzler, Fastlite). The pulse shaper is used to compress the excitation pulses and generate the pump pulse pair required for the 2D measurements. Also controlled by the pulse shaper is the time delay, τ, between the pulse pair and, most importantly, the relative phase between the pump pulses, ϕ_{12}, such that phase cycling techniques can be employed to isolate the desired signal as described above. A retroreflector mounted on a computer-controlled motorized delay stage, used to control the waiting time, T, redirects the optical path of the pump through a half-wave plate (HWP) toward an off-axis parabolic (OAP) mirror. The HWP, mounted on a computer-controlled motorized rotation stage, can be used to control the relative polarization between the pump pulses and the probe pulse if polarization-sensitive measurements are desired. Finally, the f = 25 cm silver-coated 90° OAP mirror focuses the excitation beam into the sample with a spot size of ~250 μm. Meanwhile, the output of the OPA-DFG source is passed through Ge plates used for dispersion compensation for materials in the probe path, namely, those of the sample holder. A ZnSe beam splitter is then used to generate the probe and reference beams, both of which are directed toward a f = 15 cm gold-coated 90° OAP mirror and focused into the sample with a spot size of ~150 μm. The probe and reference beams are vertically displaced such that only the probe and excitation beams are spatially overlapped. Following the sample, the IR beams are collimated with an identical OAP and focused with a f = 10 cm ZnSe lens into the slit of the spectrometer (TRIAX 190, HORIBA). The reference and probe beams are separately imaged onto one of the two 64 element HgCdTe photodiode detector arrays (InfraRed Associates), and the signal is passed through a 128-channel integrator (FPAS-0144, Infrared Systems Development) balanced to the responses of the individual HgCdTe elements. Finally, pulse-to-pulse, the probe spectrum is normalized by the reference spectrum to help minimize fluctuations in the laser power of the OPA-DFG output.

It is important to recognize that the setup described above is one specific example of the implementation of a 2DEV spectrometer. Of course, 2DEV spectroscopy can function across a range of excitation and detection conditions dependent on the light sources employed and the compatibility of pulse shaping and detection capabilities. For example, Gaynor *et al.* utilized a spectrally broadened UV pump source for the 2DEVS studies of the solar cell dye, [Ru(dcbpy)$_2$(NCS)$_2$] (dcbpy = 4,4′-dicarboxy-2,2′-bipyridine) (N3),[4,24] while Song *et al.* demonstrated a 2DEV spectrometer with excitation frequencies ranging from 490 to 950 nm.[25] In a later paper by Gaynor *et al.*, the applicability of a broadband mid-IR source

© Author(s) 2021

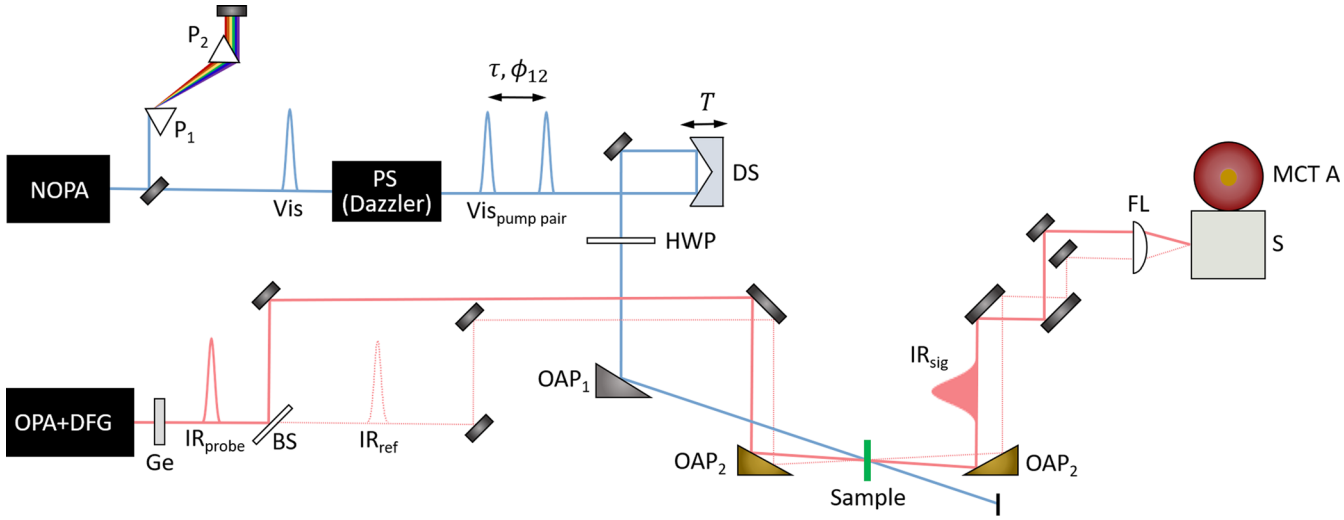

FIG. 2. Schematic of the 2DEVS experimental setup. The visible excitation beam path is shown in blue, and the IR detection (solid) and reference (dashed) paths are shown in red. The Dazzler (pulse shaper, PS) is used to control the time delay, τ, and the relative phase, φ_{12}, between the pump pair and a motorized delay stage controls the waiting time, T, between the pump pair and the IR probe. Following the light–matter interactions at the sample position, the signal is self-heterodyned via the collinear probe beam and spectrally dispersed onto the detector array. P_1 and P_2: prisms used to precompensate for the dispersion imparted by the Dazzler, PS: pulse shaper (Dazzler, Fastlite), DS: delay stage, HWP: half-wave plate, Ge: germanium plates for IR pulse compression, BS: beam splitter, OAP_1 and OAP_2: off-axis parabolic mirrors, FL: focusing lens, S: spectrometer, and MCT A: liquid nitrogen-cooled HgCdTe photodiode detector arrays.

was demonstrated;[26] however, the experimental implementation of broadband probes remains limited.

IV. THE 2DEV SPECTRUM

Two main defining features emerge as apparently unique to 2DEV spectra: (1) improved spectral resolution along *both* the electronic and vibrational axes and (2) the ability to correlate the electronic and nuclear dynamics as a function of waiting time. In order to understand how the simultaneous vibrational and electronic spectral dimensions can be utilized to understand the dynamics on complex potential energy surfaces, often necessarily in conjunction with high-level electronic structure calculations, the 2DEV study of two triphenylmethane dyes[27] will serve as our main example throughout. In this study, on crystal violet (CV) and malachite green (MG), the evolution of the vibrational structure (in the C=C aromatic stretch region) and of the 2DEV line shape as a function of waiting time allowed for changes in the molecular geometry to be mapped in order to understand the evolution on the excited state potential energy surface. In particular, the evolution of the 2DEV line shape, as characterized by the center line slope (CLS), proved to be remarkably valuable in the interpretation of the dynamics. As such, a separate section is devoted to this quantity, and in the current one, the emphasis will be placed on what these spectra actually look like.

Figure 3 serves to introduce the typical features of a 2DEV spectrum. In the spectra for CV in deuterated methanol, five peaks are evident—one with a delayed appearance at 1589 cm^{-1} [first evident in Fig. 3(e)]. Under excitation conditions—centered around the origin of the vibronic progression—that are insufficient to excite one quantum of the vibrational modes interrogated by the later light–matter interaction, stimulated emission pathways are inherently excluded.[1] Therefore, positive and negative features in the spectra are easily interpretable as vibrational evolution on the ground or excited/newly populated state, respectively [Figs. 3(g) and 3(h)]. Therefore, in Fig. 3, positive (red/green) peaks correspond to ground state bleaches, while negative (purple/blue) peaks indicate new or excited state absorptions. The ability to resolve the dynamics via 2DEVS is more apparent when the time-dependent amplitudes of these peaks are plotted (Fig. 4). It is again important to note that the ease with which these dynamics are disentangled is entirely due to the improved resolution afforded by IR detection, which is highly sensitive to changes in the molecular geometry.

Taking the case of CV in deuterated methanol and deuterated propanol as an example, the fact that the peak at 1513 cm^{-1} reaches the maximum promptly while the peak at 1577 cm^{-1} has a slower and viscosity-dependent rise suggests that the two peaks arise from differing locations on the excited state potential surface (Fig. 4). In combination with electronic structure and vibrational oscillator strength calculations, the peak at 1513 cm^{-1} was assigned to the Franck–Condon region ($S_{1,FC}$) or nearby metastable configuration, while the peak at 1577 cm^{-1} was assigned to the S_1 minimum ($S_{1,min}$). Very apparent is the delayed and viscosity-dependent appearance of the peak at 1589 cm^{-1}, which was assigned to the ground state immediately following passage through CI ($S_{0,twist}$). More explicitly, note the different timescales for the appearance of this peak for CV in methanol [Fig. 4(a)] vs in propanol [Fig. 4(c)]. In Sec. V, we will discuss how the CLS dynamics support and add to this picture.

One very important aspect of the spectra not evident in the above example is the improved frequency resolution along the electronic excitation axis. To recognize the origin of this phenomenon,

© Author(s) 2021

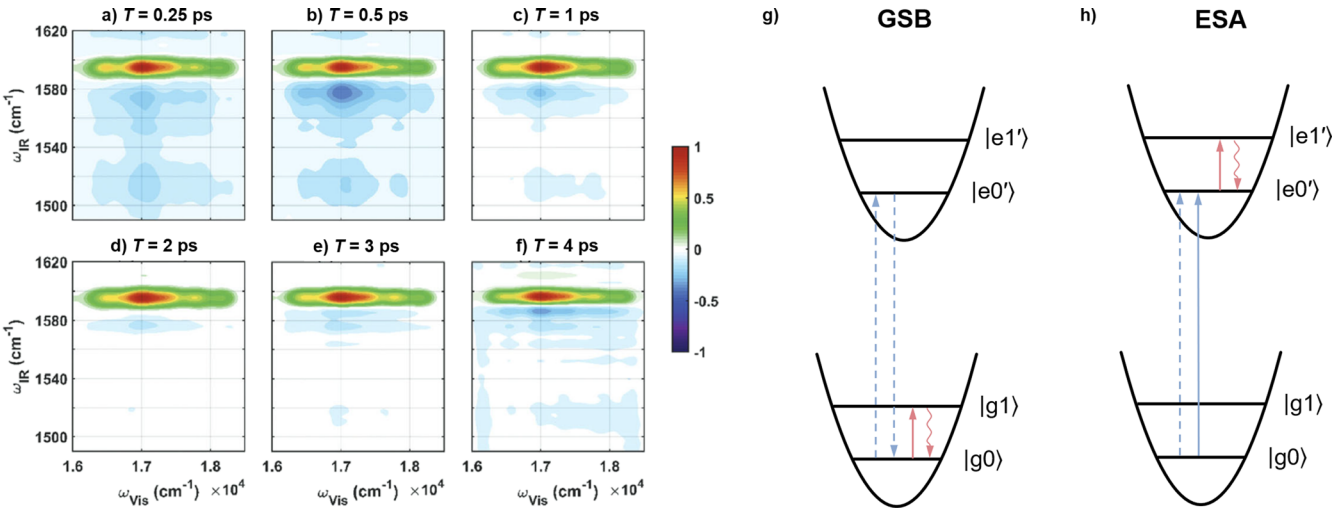

FIG. 3. (a)–(f) 2DEV spectra for crystal violet (CV) in deuterated methanol at six different waiting times.[27] Positive features indicate ground state bleaches, while negative features represent induced absorptions. The 2DEV spectra for malachite green in deuterated methanol are similar to those for CV. Reproduced with permission from Wu *et al.*, Phys. Chem. Chem. Phys. **21**, 14153 (2019). Copyright 2019 the PCCP Owner Societies. [(g) and (h)] Energy level diagrams illustrating evolution on the electronic ground or excited state, respectively.

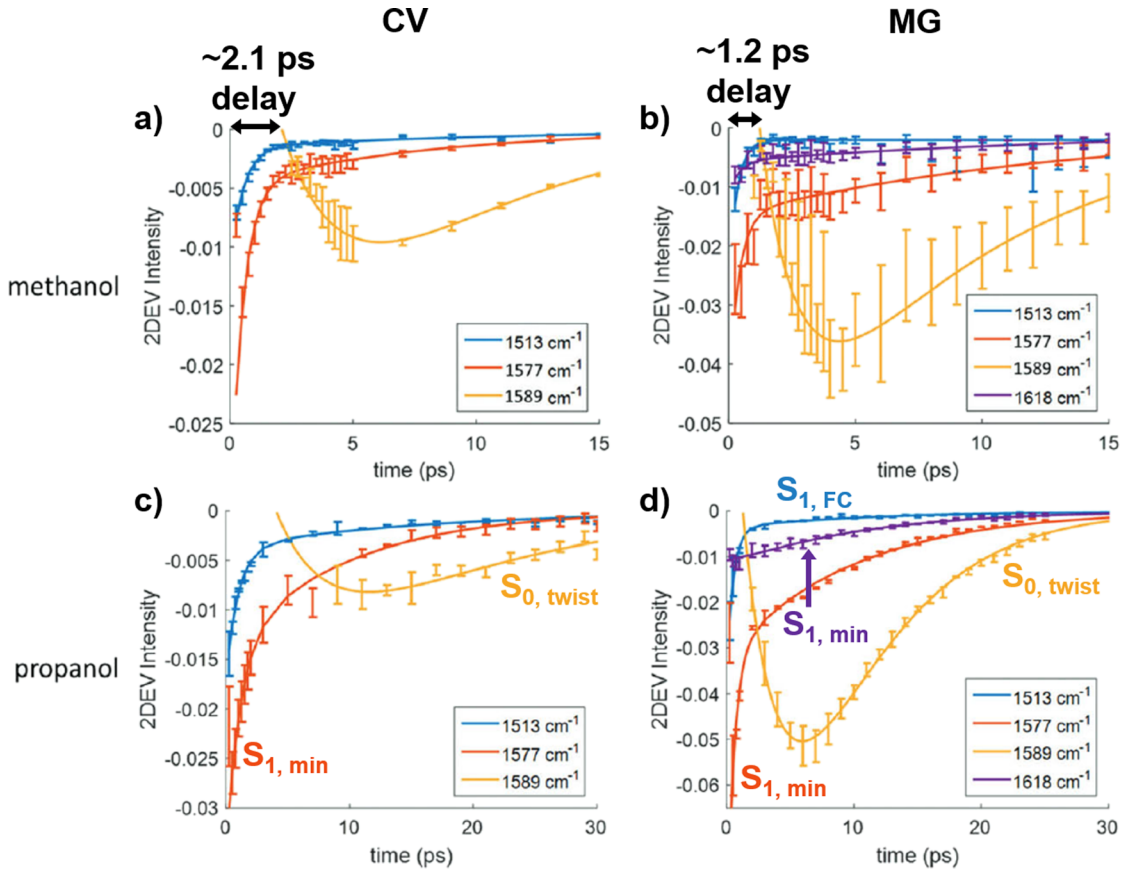

FIG. 4. Time dependence of the 2DEV features at particular IR detection frequencies of crystal violet (CV) (left) and malachite green (MG) (right). Also shown is the solvent dependence of CV and MG in deuterated methanol [(a) and (b)] and deuterated propanol [(c) and (d)]. The solid lines represent bi-exponential fits to the data. Note the change in the scale of the time axis between solvents. Reproduced with permission from Wu *et al.*, Phys. Chem. Chem. Phys. **21**, 14153 (2019). Copyright 2019 the PCCP Owner Societies.

© Author(s) 2021

it is necessary to consider that the requirement for observing a peak in a 2DEV spectrum is that the conditional probability $P(\omega_e;\omega_v)$ is non-zero, where ω_e is the electronic excitation energy and ω_v is the vibrational detection frequency. The consequence of this highly specific condition manifests significantly in systems with multiple closely-lying electronic/vibronic states. In such systems, there is often a certain degree of spectral congestion as a result of the many closely spaced levels, which makes resolving them difficult with electronic spectroscopies where the conditional probability $P(\omega_e;\omega_{e'})$ (where ω_e is the electronic excitation energy and $\omega_{e'}$ is the electronic detection frequency) is comparatively more relaxed. A graphical demonstration of the effect of the condition $P(\omega_e;\omega_v)$ is shown in Fig. 5 where there is a noticeable enhancement of the spectral resolution in the 2DEV spectrum along the excitation axis [Figs. 5(b)–5(d)] vs the corresponding linear absorption spectrum [Fig. 5(a)] where states ε_1–ε_4 are indistinguishable. While it is more obvious that IR detection allows for the signatures of various electronic states to be dispersed along the detection axis as a result of the vibrational frequency dependence on the given electronic manifold [2DEVS features pointed out with the black arrow in Fig. 5(b)], this is not necessarily the cause of enhanced resolution along the excitation axis. Rather, this enhancement can occur even if there is little difference in the characteristic vibrational frequencies of given electronic/vibronic states. Such a phenomenon is highlighted in Figs. 5(c) and 5(d), which show slices through the 2DEV spectrum

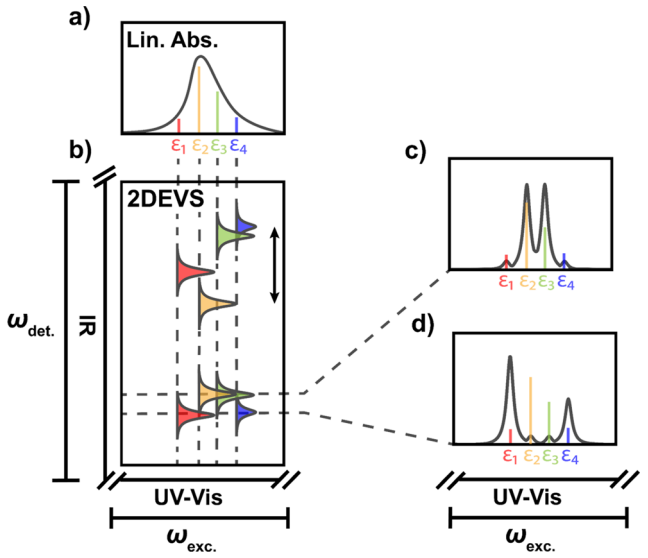

FIG. 5. (a) Representative linear absorption spectrum for a system with many closely space, unresolvable, electronic/vibronic levels labeled ε_1–ε_4. (b) Associated cartoon 2DEV spectrum depicting the dependence of the detected vibrational structure on the given electronic state, which can vary substantially (see the top portion highlighted with the black arrow to show the frequency spread) or only slightly (see the bottom portion of the spectrum). [(c) and (d)] Slices through the 2DEV spectrum at a fixed detection frequency emphasizing the improved frequency resolution along the excitation axis. Also shown in is how the dependence of features on both the electronic and vibrational transition moments can amplify certain states with respect to the linear absorption spectrum (see the intensity of the red vs blue features).

at fixed detection frequencies. In this case, the condition $P(\omega_e;\omega_v)$ essentially results in a gap between 2DEVS peaks.

In practice, this effect is not always quite as dramatic; however, it is still striking. Figure 6 shows the 2DEV spectra of light-harvesting complex II (LHCII) under various excitation conditions. For example, Fig. 6(b) shows that there is a clear separation between chlorophyll (Chl) *a* and Chl *b* excitation frequencies, at 14 800 and 15 500 cm^{-1}, respectively, in the 2DEV spectrum, while the absorption spectrum, even at 77 K, does not show a clear minimum between the two peaks [Fig. 6(a)]. Even more striking in the 2DEV spectrum is the region between 17 500 and 19 000 cm^{-1}, which shows clear structure [Figs. 6(c)–6(f)], while the electronic absorption spectrum in this region is entirely devoid of discernable features [Fig. 6(a)].[19] The same phenomenon was also prevalent in 2DEVS studies of N3 where distinct spectral bands corresponding to different MLCT states were observed despite a broad and overwhelmingly featureless linear absorption spectrum (Fig. 7).[4,24] In this case, simultaneous high spectral resolution along both the electronic and vibrational dimensions was necessary to understand how vibronic couplings mapped across multiple electronic states, as well as high- and low-frequency vibrations, were all implicated in the CT process of this system.[4] In fact, it was the spectral resolution capabilities of 2DEVS that allowed this study to be the first to demonstrate the utilization of multidimensional spectroscopy to describe molecular eigenstates in terms of three energetically disparate molecular DoF. Yet, more remarkable was how the clearly resolved distinct MLCT states allowed for a direct insight into the propagation of excited-state vibronic coherences accompanying nonadiabatic internal conversion—providing an unequivocal view of the underlying mechanism driving long-lived charge separation in this system. All these examples highlight how 2DEV spectra can provide detailed information in regions that are devoid of structure in electronic absorption spectra.

V. THE CENTER LINE SLOPE

In many cases, the ability of 2DEV spectra to correlate the electronic and nuclear dynamics as a function of waiting time is the defining factor that allows for connections to be drawn between spectroscopic observables and the actual underling photochemical or photophysical mechanism(s) of a system. For example, 2DEVS studies of the excited state deactivation of the triphenylmethane dyes, CV and MG, relied heavily on changes in the 2D line shape to understand the dynamics surrounding a conical intersection (CI). In addition, this electronic–nuclear correlation proved essential to understanding the solvent-dependent excited state proton transfer process of indigo carmine,[28] as well as the degree of concertedness in a biomimetic proton-coupled electron transfer (PCET) system.[29] In all these studies, it was clear that transient IR experiments alone lacked the detail necessary to map out potential surfaces or to understand the role of solvent.

The theory underpinning the description of the CLS as representing a cross correlation of the fluctuating parts of the electronic and vibrational energy gaps for individual molecules in solution has recently been developed by Cho and Fleming.[17] In this case, the CLSs for the ground state bleach (GSB) and the excited state absorption (ESA) are given by

© Author(s) 2021

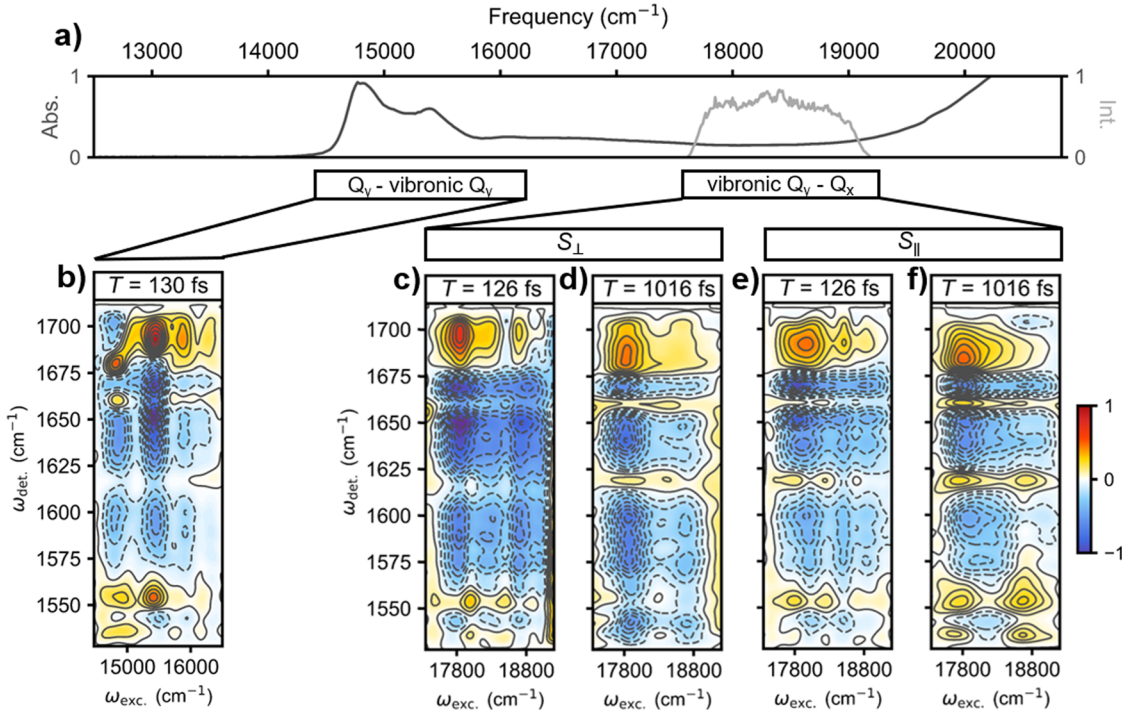

FIG. 6. (a) Linear absorption spectrum of LHCII at 77 K, along with the spectrum of the visible pump pulses employed in the experiment. (b) Representative 2DEV spectrum of the Q_y bands of LHCII at $T = 130$ fs, prior to significant Chl *b* to Chl *a* transfer. Ground state bleach features are positive (red), and excited state absorption features are negative (blue). [(c) and (d)] Perpendicular polarization-associated (PA) 2DEV spectra of the vibronic Q_y–Q_x bands of LHCII at 77 K. [(e) and (f)] Parallel PA 2DEV spectra of the vibronic Q_y–Q_x bands of LHCII at 77 K. Reproduced with permission from Arsenault *et al.*, Nat. Commun. **11**, 6011 (2020). Copyright 2020 Author(s), licensed under a Creative Commons Attribution 4.0 License.

$$\mathrm{CLS}_{\mathrm{GSB}}(T) = \frac{\langle \delta\omega_{\mathrm{eg}}(T)\delta\omega_{\mathrm{gg}'}(0)\rangle}{\langle \delta\omega_{\mathrm{eg}}{}^2\rangle} \tag{7}$$

and

$$\mathrm{CLS}_{\mathrm{ESA}}(T) = \frac{\langle \delta\omega_{\mathrm{eg}}(T)\delta\omega_{\mathrm{ee}'}(0)\rangle}{\langle \delta\omega_{\mathrm{eg}}{}^2\rangle}, \tag{8}$$

where subscripts gg′ and ee′ refer to vibrational excitation frequencies in the ground and excited states, respectively. These expressions describe the correlation of the electronic and vibrational frequencies via coupling of their transition frequencies to the same solvent motions. If the solvent–solute interaction can be described by the interaction of the solute dipole moment and the solvent electric field,

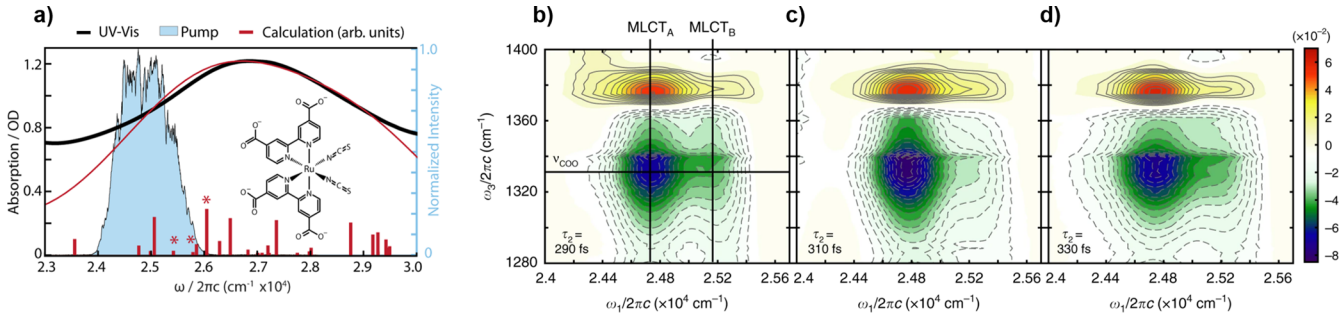

FIG. 7. (a) Electronic absorption spectrum of N3 in basic, aqueous solution (pH 13) (black) along with the spectrally broadened UV pump spectrum (blue). The calculated (TD-B3LYP/def2-SVP) electronic absorption spectrum (with a Gaussian broadening applied) is also shown (red) along with the predicted $S_0 \rightarrow S_n$ oscillator strengths (red sticks). Reproduced with permission from Gaynor *et al.*, J. Chem. Phys. Lett. **9**, 6289 (2018). Copyright 2018 American Chemical Society. [(b)–(d)] 2DEV spectra of N3 at various waiting times. Ground state bleach features are positive (red/yellow), and excited state absorption features are negative (blue/green). Assignments are shown in (b) where the MLCT transitions along with the high-frequency detection mode have been labeled. Reproduced with permission from J. D. Gaynor, J. Sandwisch, and M. Khalil, Nat. Commun. **10**, 5621 (2019). Copyright 2019 Author(s), licensed under a Creative Commons Attribution 4.0 License.

© Author(s) 2021

then the fluctuating part of the potential energy difference is given by

$$\delta V_{eg}(q) = -\Delta\mu_{eg} \cdot E_{solvent}(q), \tag{9}$$

where q is the bath coordinate and $\Delta\mu_{eg} = \mu_e - \mu_g$ is the difference in dipole moment between the excited and ground electronic states. Similarly, for the vibrational Stark effect, the vibration frequencies will fluctuate as follows:

$$\delta F_i V_i(q) = -\delta\mu_i \cdot E_{solvent}(q), \tag{10}$$

where i = e, g such that $\delta\mu_i$ is the vibrational Stark tuning rate of the jth normal mode in the ground or excited electronic state. Here, the F operators connect the solvent–solute interaction to the frequency shifts of the specific modes. With these various approximations in place, the cross correlation functions in (7) and (8) can be simplified to[17]

$$\langle \delta\omega_{eg}(T)\delta\omega_{gg'}(0)\rangle = \langle E_{solvent}(q(T))\{\Delta\mu_{eg}(T)\delta\mu_g(0)\} \cdot E_{solvent}(q(0))\rangle/\hbar^2 \tag{11}$$

and

$$\langle \delta\omega_{eg}(T)\delta\omega_{ee'}(0)\rangle = \langle E_{solvent}(q(T))\{\Delta\mu_{eg}(T)\delta\mu_e(0)\} \cdot E_{solvent}(q(0))\rangle/\hbar^2. \tag{12}$$

The quantities $\Delta\mu_{eg}\delta\mu_g$ and $\Delta\mu_{eg}\delta\mu_e$ are dyadic products of the two vector Stark tuning rates.

Within this formalism, we can understand how correlations between the electronic and vibrational DoF manifest in the 2D line shape. Figure 8 contains cartoon representations of how various relations between $\delta\mu_e$ (where we note this example is for an excited state vibration) and $\Delta\mu_{eg}$ can drive the CLS dynamics. For example, Fig. 8(a) illustrates the most straightforward dynamical case when solvation dynamics, driven by $\delta\mu_e$, dominate. Observing this CLS behavior is expected mainly in unreactive systems, when changes in $\Delta\mu_{eg}$ will not overwhelm the electronic–nuclear correlation. An experimental example of this case is shown in Fig. 9 for dye 3,3′-diethylthiatricarbocyanine iodide (DTTCI).[16] As expected, the CLS decays exponentially to zero on a timescale of ~1.6 ps, which matches the vibrational dephasing time.

However, the more interesting scenarios are rather when $\Delta\mu_{eg}$ is the prevailing influence over the correlation [Figs. 8(b) and 8(c)]. Starting with Fig. 8(b), this cartoon depicts how a gradual increase in $\Delta\mu_{eg}$ results in an increase in the CLS. For clarity of the illustration, $\delta\mu_e$ is shown not to vary, but this is a noted simplification. Regardless, it now becomes clear how changes in the 2DEVS line shape for reactive systems can be utilized to connect spectroscopic dynamics (e.g., peak amplitudes) with the underlying mechanistic function of the system. For example, the CLS dynamics, in addition to high-level computational modeling, were crucial to understanding ultrafast photoinduced PCET in a biomimetic system, benzimidazole-phenol-pentafluorophenylporphyrin ($BIPPF_{15}$) (Fig. 10).[29] In this example, a 120 fs rise in the CLS was observed [Fig. 10(a)], indicating an increasing electronic–nuclear correlation. With the aid of electronic structure calculations, it was found that while there was a little change in the electronic density distribution between the ground state and the locally excited state [LE, Fig. 10(b)], there was a substantial change in the distribution for the proton and electron transferred state [PET, Fig. 10(c)]. The significant difference between the electron density distribution of the PET state vs that of both the ground state potential energy surface and the LE state, therefore, indicated the emergence of a large electric dipole moment in the PET state (and a corresponding change in the solvent configuration). To further interpret the evolution of the CLS, the dipole moment of the PET state was calculated as a function of the dihedral angle to track the evolution from the LE to PET state [Fig. 10(d)]. With the result showing a continual increase in the dipole moment, the rise in the CLS was understood as being driven by charge

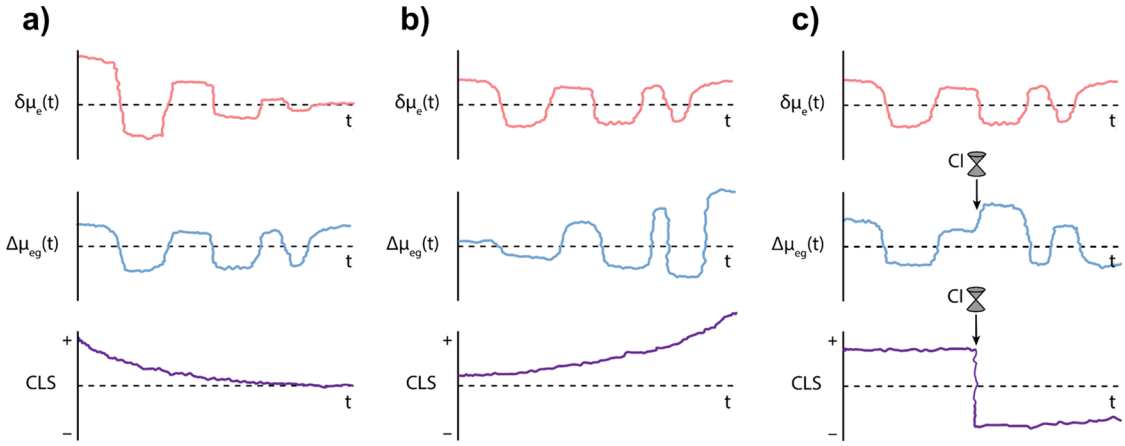

FIG. 8. Illustration of the origins of various forms of center line slope (CLS) evolution, in this case for an excited state absorption feature, guided by the formalism presented in Ref. 17. Correlations between the fluctuations of $\delta\mu_e$ and $\Delta\mu_{eg}$ are shown when (a) $\delta\mu_e$ dominates leading to an exponential decay in the CLS indicative of vibrational dephasing; (b) $\Delta\mu_{eg}$ dominates as a result of electronic structure evolution, for example, which can lead to an exponential rise or decay and be positive or negative (the example above is for the scenario when $\Delta\mu_{eg}$ increases and the correlation is positive); and (c) when a sudden change in $\Delta\mu_{eg}$ occurs as a result of a relaxation through a conical intersection (CI), for example (the illustrated example is for the case when the electronic dipole moment reverses direction above and below the CI).

© Author(s) 2021

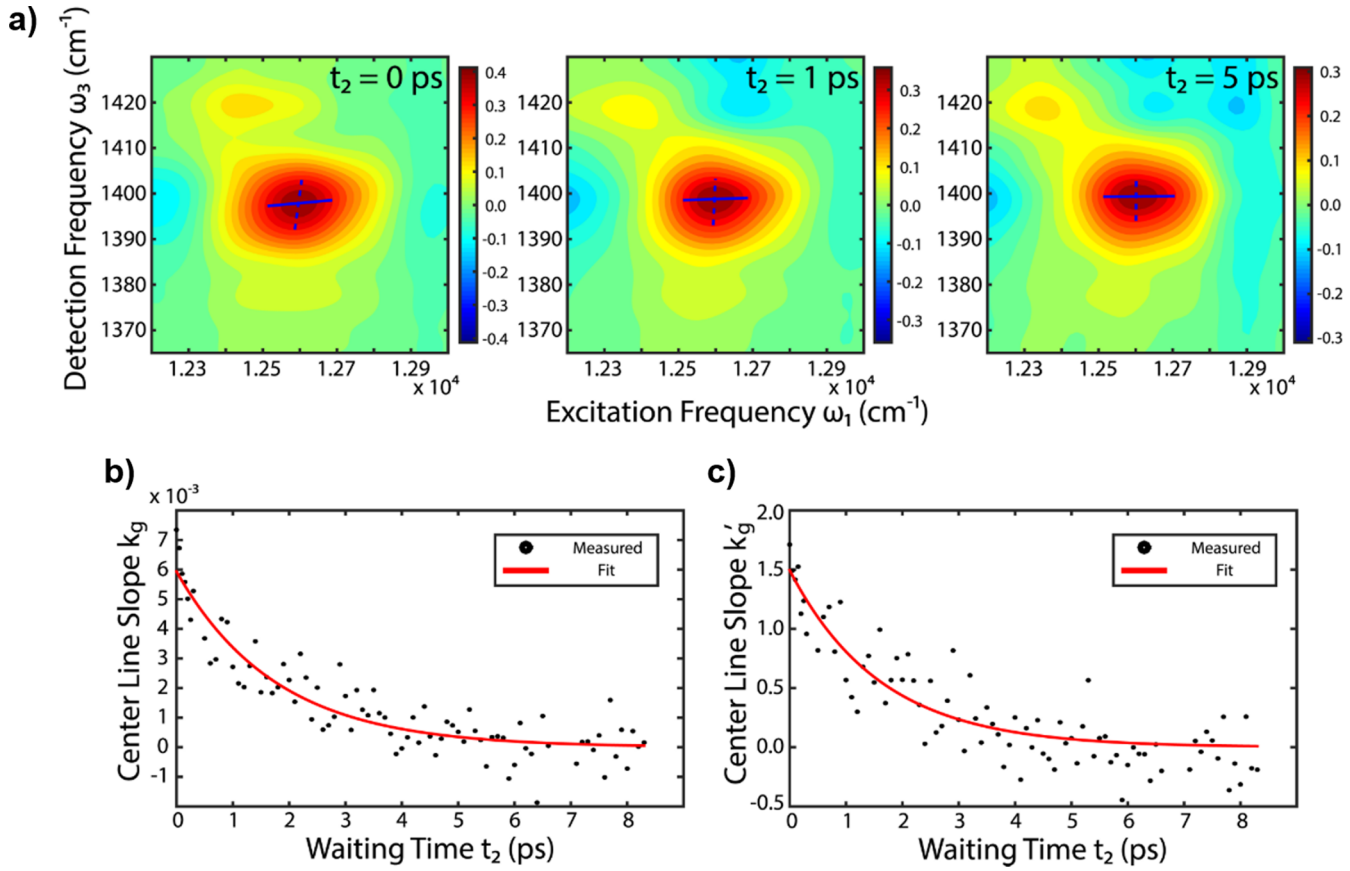

FIG. 9. (a) Evolution of a single ground state bleach peak in the 2DEV spectrum of DTTCI in $CDCl_3$ at various waiting times.[16] (b) CLS of the peak obtained vs the electronic frequency axis. (c) CLS of the peak vs the IR frequency axis. Both plots give the same decay time of ~1.6 ps. Reproduced from Lewis *et al.*, J. Chem. Phys. **142**, 174202 (2015) with the permission of AIP Publishing.

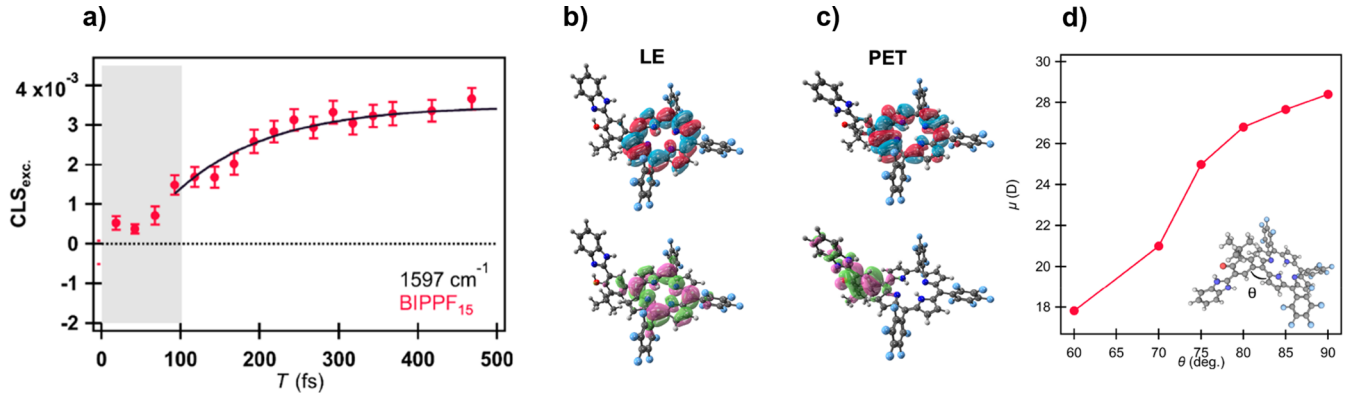

FIG. 10. (a) CLS dynamics for a selected 2DEV feature of the biomimetic system $BIPPF_{15}$. The time range where visible and IR pulses overlap, <100 fs, is indicated by the shaded area, the error bars show the standard error of the CLS, and the black curve indicates the fit result of the CLS dynamics with a single exponential function (a rise of 120 ± 20 fs). [(b) and (c)] The dominant NTO pairs for locally excited (LE) and proton and electron transferred (PET) states of $BIPPF_{15}$, respectively. For each state, the highest occupied NTO is on the bottom and the lowest occupied NTO is on the top. (d) Calculated dipole moment of $BIPPF_{15}$ as a function of dihedral angle between BIP and porphyrin moieties. The optimized structure of the PET state of $BIPPF_{15}$ is also shown in the inset. Reproduced with permission from Yoneda *et al.*, J. Am. Chem. Soc. **143**, 3104 (2021). Copyright 2021 American Chemical Society.

© Author(s) 2021

redistribution concomitant with dihedral angle twisting, leading to the formation of a substantial dipole moment. This observation showed that the electron transfer component of PCET cannot be described as a single kinetic step—a subtlety not apparent in the parallel transient IR experiment, which was unsurprisingly not sensitive to the synergistic molecular motions.

Finally, we will consider the last example of how a change in $\Delta\mu_{eg}$ as a result of rapid radiationless relaxation (i.e., involving a CI) can influence both the sign and magnitude of the CLS. An illustration of this phenomenon is shown in Fig. 8(c). A change in the sign of the CLS can occur when there is a reversal in the dipole moment as a result of significant nuclear rearrangement.[27,28] This sensitivity to the molecular geometry along a potential surface is again a significant advantage when the goal is to understand condensed phase molecular dynamics. Returning to the example of the triphenylmethane dyes, this was exactly the type of CLS behavior observed (Fig. 11).[27] For CV, the CLS for the $S_{o,eq}$ band was positive (after ~3 ps, the CLS becomes negative as a result of overlap with the new $S_{0,twist}$ band), while the CLS of the $S_{1,min}$ band was immediately negative. The comparison between the negative CLS of the $S_{1,min}$ band vs the positive CLS of the $S_{0,twist}$ band is even more striking—especially in contrast with the CLS dynamics of MG where no such sign changes are apparent. When compared to electronic structure calculations, the interpretation of these results becomes quite clear. For CV, there is a reversal in the molecular dipole moment between the $S_{1,min}$ and the $S_{0,twist}$ geometries, while for MG, the direction of the dipole moment remains unchanged above and below the CI. Figure 12 contains a schematic summary of the photoinduced excited state evolution and radiationless deactivation of CV using dominant natural transition orbitals (NTOs)[30] as understood via the CLS dynamics.

VI. COUPLED SYSTEMS

Up to this point, the 2DEV spectrum, while revealing, has been shown to be straightforward in appearance. However, when multiple molecules are electronically or vibronically coupled, the appearance and evolution of the 2DEV spectrum are somewhat less intuitive. Here, we will explicitly consider coupled systems that undergo ET. In order to understand how this phenomenon can manifest in 2DEVS, recall that the condition for observing a peak in a 2DEV spectrum is that the conditional probability $P(\omega_e;\omega_v)$ is nonzero, whereas, in 2D electronic spectra, the necessary condition is, instead, that $P(\omega_e;\omega_{e'})$ is nonzero. In 2DES, the growth of cross peaks corresponding to lower energy diagonal features as a result of ET is well-known and intuitively clear.[31] However, in 2DEVS, when ET

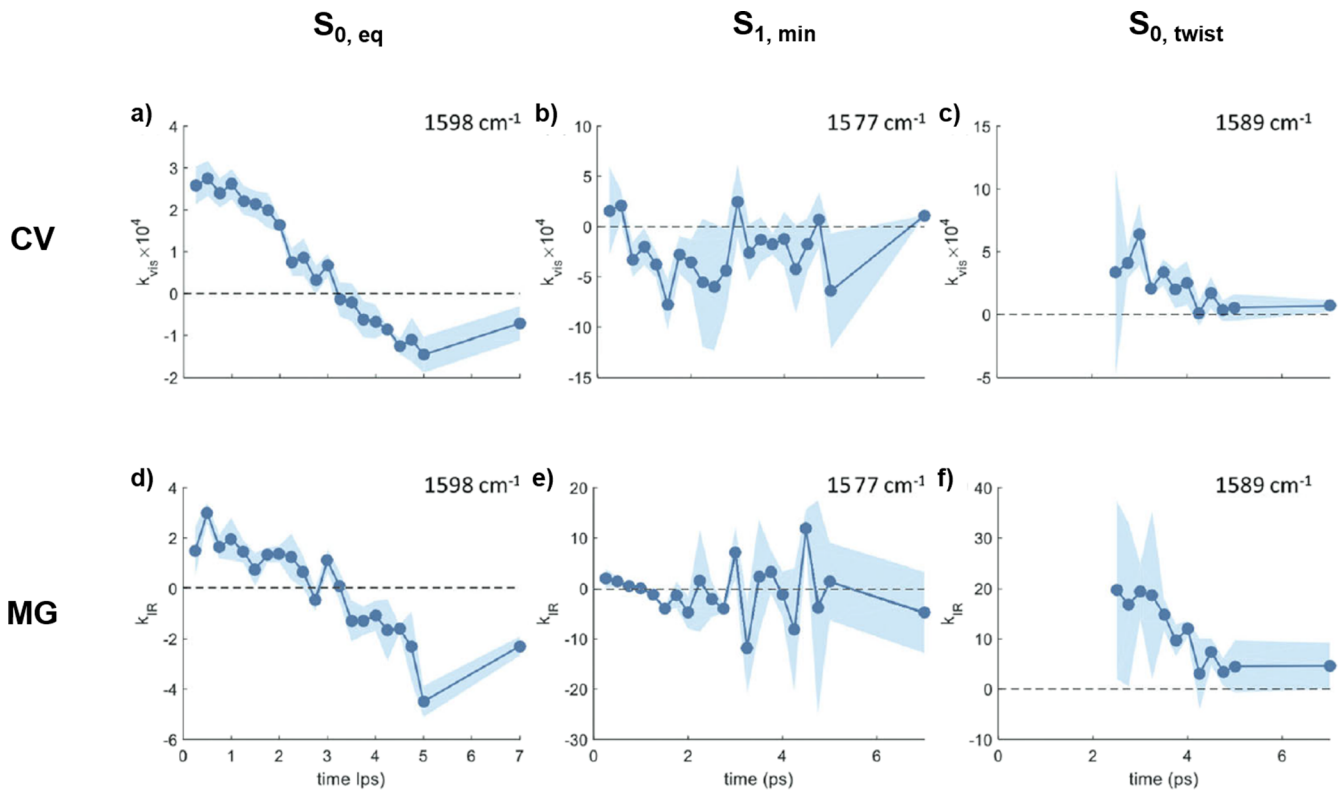

FIG. 11. CLSs for crystal violet (CV) [(a)–(c)] and malachite green (MG) [(d)–(f)] in deuterated methanol for the bands as indicated in the plots. The shaded region represents the standard error. Reproduced with permission from Wu *et al.*, Phys. Chem. Chem. Phys. **21**, 14153 (2019). Copyright 2019 the PCCP Owner Societies.

© Author(s) 2021

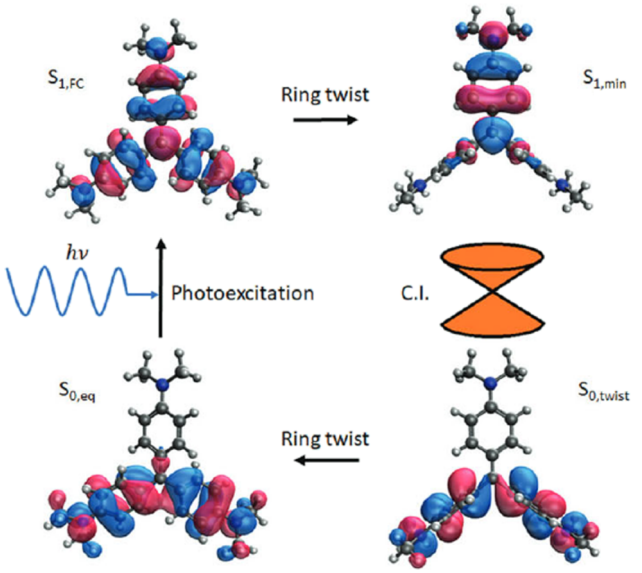

FIG. 12. A cartoon illustrating the photoinduced excitation, subsequent evolution, and ultimate radiationless decay through the conical intersection of crystal violet. The orbitals pictured are the dominant virtual NTOs for $S_{1,FC}$ and $S_{1,min}$ and the dominant occupied NTOs for $S_{0,eq}$ and $S_{0,twist}$. Reproduced with permission from Wu *et al.*, Phys. Chem. Chem. Phys. **21**, 14153 (2019). Copyright 2019 the PCCP Owner Societies.

occurs, the spectrum becomes increasingly symmetric along the excitation axis as peaks corresponding to $P(\omega_{e_\beta};\omega_{v_\beta})$ begin to decay, while peaks corresponding to $P(\omega_{e_\alpha};\omega_{v_\alpha})$ gain amplitude—notably at positions $P(\omega_{e_\beta};\omega_{v_\alpha})$—through the transfer.[2,3] Here, α and β signify two excitonic states, for example, where $\omega_{e_\alpha} > \omega_{e_\beta}$.

The simplest model to capture the effects of ET in 2DEVS consists of two electronically coupled monomers, A and B, each with one electronic and one vibrational DoF. Furthermore, the vibrational DoF are treated as localized modes (small Huang–Rhys factor), which retain site-specificity. The electronic coupling, J, therefore, results in the formation of excitonic states with mainly electronic character. This model, although straightforward, already contains nine excitonic states: a ground electronic state, two excited excitonic states, and two vibrational levels in each manifold. In this section, we will present two different calculations based on this model: one is more general that is useful to understand the spectral evolution and role of J, while the other is slightly more specific to LHCII and proved to be highly valuable in understanding the corresponding experimental results. In Fig. 13, we show the calculated spectra for a dimer that supports ET as described above.[32] When the coupling is weak, the resulting excitonic states are hardly mixed and an excitation of exciton ν (of mainly B character), for example, produces essentially no vibrational signal characteristic of A at short times. However, as T increases, the spectra become increasingly symmetric—rather than solely B features (mostly contributing to ν) decreasing, new features characteristic of the lower excitonic state, μ, will *appear*. More explicitly, bands along the excitation axis indicate what states were initially populated. As ET occurs during the waiting time, population can transfer from ν to μ such that a vibration specific to the μ manifold will grow along the detection axis. In the case of stronger coupling, the mixing of A and B is more pronounced and apparent in the spectra even at $T = 0$ fs [Fig. 13(d)]. The increasing degree of symmetry between excitonic bands as the waiting time evolves is also apparent in this case. The important implication for the spectral evolution portrayed by this model is that because the vibrations are localized, they can serve as spatial proxies for the excitation. In other words, the 2DEVS dynamics reveal how excitation redistributes in space.

As 2DEVS is a direct reporter on both electronic and vibrational DoF, a strongly vibronically coupled system, such as a molecular dimer with strong electronic coupling (far exceeding that from the previous example), can dramatically alter the appearance of the spectrum and requires a number of new factors to be considered during interpretation.[33] First, the initial populations of the various exciton levels will vary strongly with only the nearly pure electronic levels and (near) resonant vibronic level(s) carrying significant oscillator strength. Second, for the third and fourth light–matter interactions, the IR transition moments must be considered carefully. For example, IR transitions that are mostly within one molecule will be significantly stronger than those involving "cross-molecule" (or "inter-site") excitation. However, a resonant vibration can promote vibronic mixing between states localized on different monomers. The vibronic mixing also enhances the cross-transition IR dipole moments for transitions between mixed vibronic states and allows the IR pulse to excite/de-excite to a state with a higher/lower vibrational quantum. Cross-transitions across mixed vibronic states formed from different monomers, therefore, become allowed. As a result, the number of pathways that contributes to the 2DEV spectrum increases. Stimulated emission (SE) pathways become allowed, in addition to the GSB and ESA pathways. Due to resonance-induced vibronic mixing, the dimeric states excited by the initial two visible pulses may not be strictly electronic. If the states have vibronic character, the third IR pulse has the capability to induce stimulated emission to a state with a lower vibrational quantum, in addition to ESA pathways where the IR pulse induces an excitation to a state with a higher vibrational quantum. In this case, assigning features in the 2DEV spectrum solely based on their sign will not always be correct.[33] In addition, weak optical transitions that might not be discernable in the linear electronic spectrum or in a 2D electronic spectrum can become evident in a 2DEV spectrum via amplification through IR transition moments. Furthermore, relaxation pathways induced by vibronic coupling to the phonon bath must be considered. The combination of all these factors must be carefully considered in order to analyze the 2DEV spectra of a strongly coupled vibronic system.

To date, no such strongly coupled system has been investigated; rather, the focus has been on the photosynthetic light-harvesting complex, LHCII. First investigated by Lewis *et al.*, the 2DEV spectra of LHCII held a remarkable level of detail about the relaxation pathways involved in ET and provided the first step toward connecting the evolution in energy space to that in physical space.[2] However, the substantial number of pigments (and therefore possible interactions) made a comprehensive understanding of all the spectral features difficult. In a later study, the emphasis was placed on the subpicosecond dynamics of LHCII in order to understand in greater detail how ultrafast energy flow spatially

© Author(s) 2021

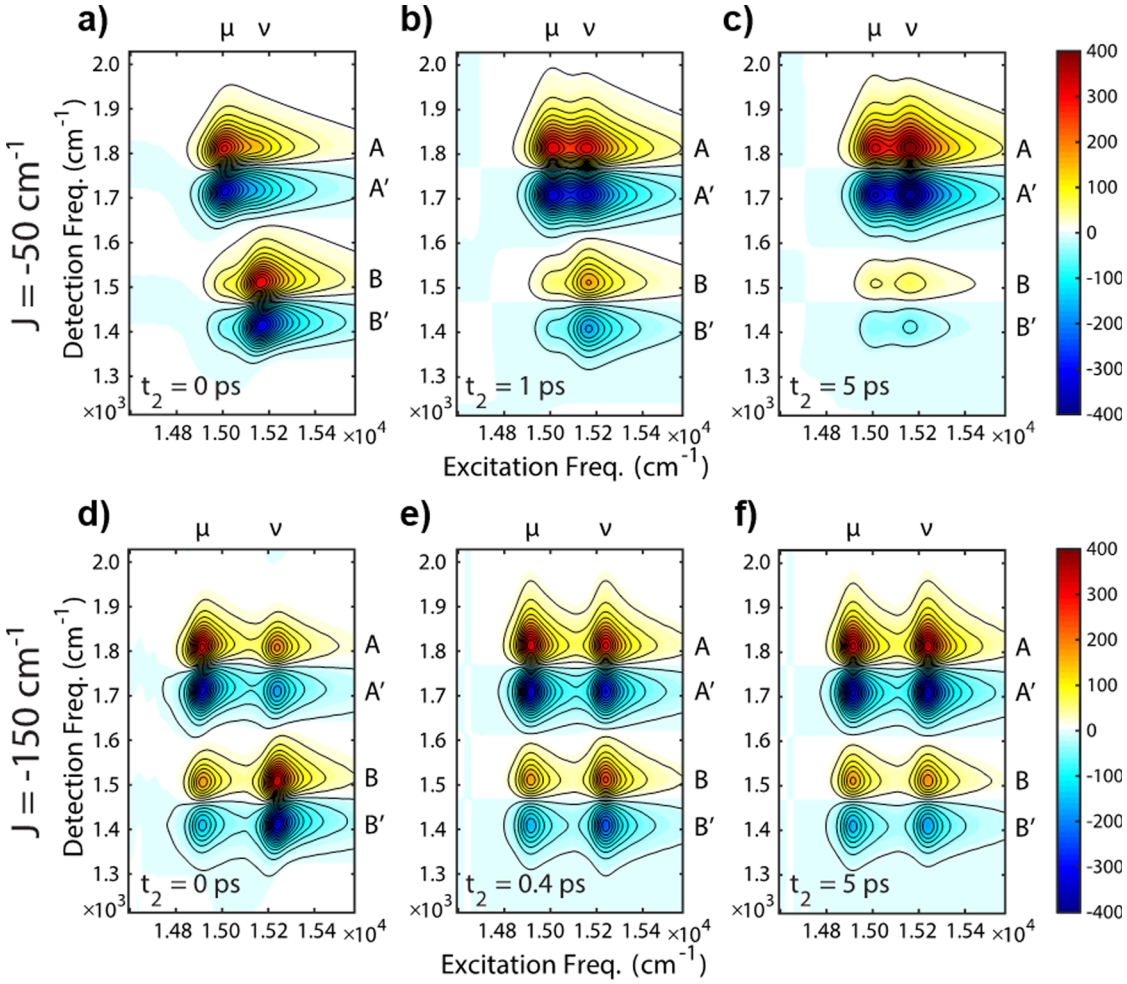

FIG. 13. Model calculations exploring energy transfer in a dimer consisting of electronically coupled monomers A and B, giving rise to two excitons, μ and ν. Positive features indicate ground state bleaches, and negative features indicate excited state absorptions (where the prime additionally indicates vibrational frequencies in the excited state). [(a)–(c)] Electronic coupling strength of $J = 50$ cm^{-1} and [(d)–(f)] $J = 150$ cm^{-1}. Reproduced from Lewis *et al.*, J. Chem. Phys. **143**, 124203 (2015) with the permission of AIP Publishing.

redistributes throughout the complex.[3] Figure 14 shows the evolution of the 2DEV spectrum of LHCII where, even on a subpicosecond timescale, the increasing degree of symmetry across the excitation axis is apparent. In addition to the mainly Chl *a* and *b* excitonic bands (14 800 and 15 500 cm^{-1}, respectively), two other bands >15 600 cm^{-1}, assigned to vibronic states of mainly Chl *b*, are noticeably present. Actually, the evolution of these bands reflects ultrafast vibronic energy flow to the lower-lying Chl excitonic states as they too become increasingly symmetric throughout the waiting time. In this study, both the peak amplitudes [Fig. 14(e)] and the CLS dynamics (Fig. 15) revealed distinct oscillatory behavior.

In order to further understand this behavior, theoretical treatment was necessary. Particularly, in contrast to the CLS dynamics of a single molecular system, the calculation of the CLS behavior of coupled molecular systems is sufficiently complex that a more insight is gained via numerical simulations of specific models. Figure 16 shows the calculated 2DEV spectrum and CLS dynamics of four ESA features of a model heterodimer, which follows a similar framework to the one previously described.[3] A comparison of the experimental LHCII spectra with the calculated spectra shows how the coupling results in the emergence of two ESA quartets—each with specific ratios of site character. Additionally, the model again shows an increasing degree of symmetry between bands throughout the waiting time, which is characteristic of ET. The model calculations also exhibit oscillatory dynamics as shown in the CLS evolution [Figs. 16(d) and 16(f)] arising from transfer between the $|B\rangle$ and $|A\rangle$ excitons (not to be confused with the A and B site labels for a previous model)—made unmistakable by the correspondence of the cross-power oscillation

© Author(s) 2021

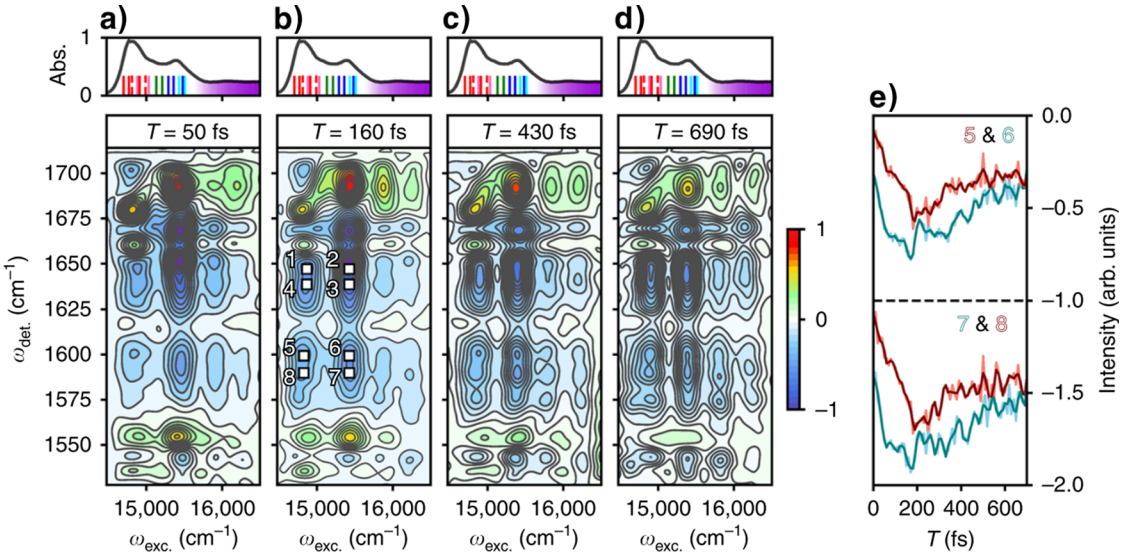

FIG. 14. (a)–(d) 2DEV spectra of LHCII at various waiting times. Positive features indicate ground state bleaches, and negative features indicate excited state absorptions (ESAs). The region of the linear absorption spectrum of LHCII (at 77 K) that was excited during this experiment has been placed at the top of each of the 2DEV spectra. The grouping of red and pink lines distinguishes the excitonic band of mainly Chl *a* character, while the grouping of blue lines distinguishes the excitonic band of mainly Chl *b* character. The purple continuum highlights the region of the absorption spectrum composed of the higher-lying vibronic states of mixed Chl character. In (b), the two ESA quartets are labeled. (e) Example of the observed oscillatory peak amplitudes, for ESAs five through eight. The peak amplitude dynamics for seven and eight have been offset for clarity. The unfiltered intensities are shown in light red and blue, while the data in dark red and blue are subjected to a 1200 cm^{-1} cutoff filter, in order to highlight the lower frequency oscillations of interest. Reproduced with permission from Arsenault *et al.*, Nat. Commun. **11**, 1460 (2020). Copyright 2020 Author(s), licensed under a Creative Commons Attribution 4.0 License.

frequency [Fig. 16(e)] matching the $|B\rangle$–$|A\rangle$ energy gap. This, in turn, enables a frequency beat map to be constructed [Fig. 16(g)] in which the correspondence of the beat frequency with the excitation frequency of the two components of the heterodimer is apparent. In more complex systems, such as the LHCII trimer with 42 Chl molecules,[34] these types of beat maps, though considerably more complex than shown in Figs. 16(e) and 16(g), explicitly map which vibrational frequencies are involved in the relaxation between specific excitons within the excitonic manifold.[3] The major advantage of utilizing the CLS when characterizing ET is that, in contrast to the amplitude of cross peaks, the CLS does not contain population dynamics. Rather, the CLS reports on a correlation, making the extraction of beat frequencies significantly more straightforward.

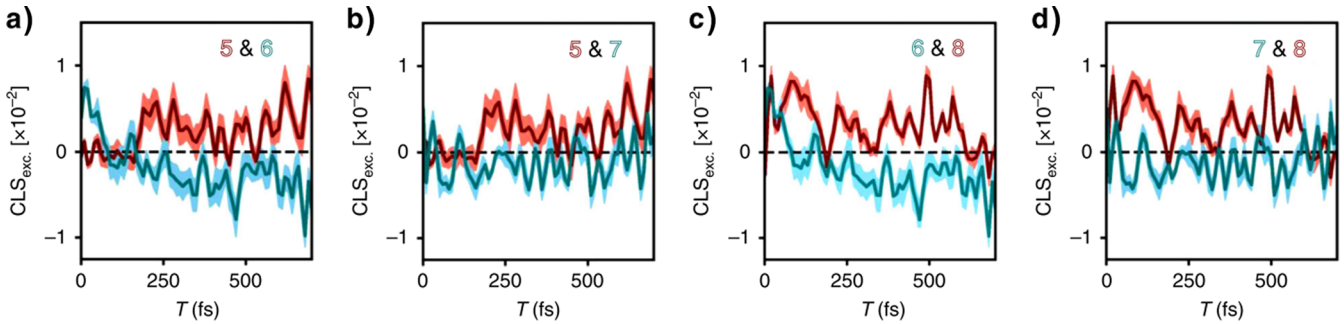

FIG. 15. Time domain center line slope (CLS) dynamics along the excitation axis of features five through eight (as labeled in Fig. 14). Pairings have been made to emphasize the clear complementary behavior. The CLSs are colored according to the peak labels in the top right corner of each plot. Shaded light red or blue regions around each CLS indicate the standard error from the linear fits used to calculate $CLS_{exc.}$. Reproduced with permission from Arsenault *et al.*, Nat. Commun. **11**, 1460 (2020). Copyright 2020 Author(s), licensed under a Creative Commons Attribution 4.0 License.

© Author(s) 2021

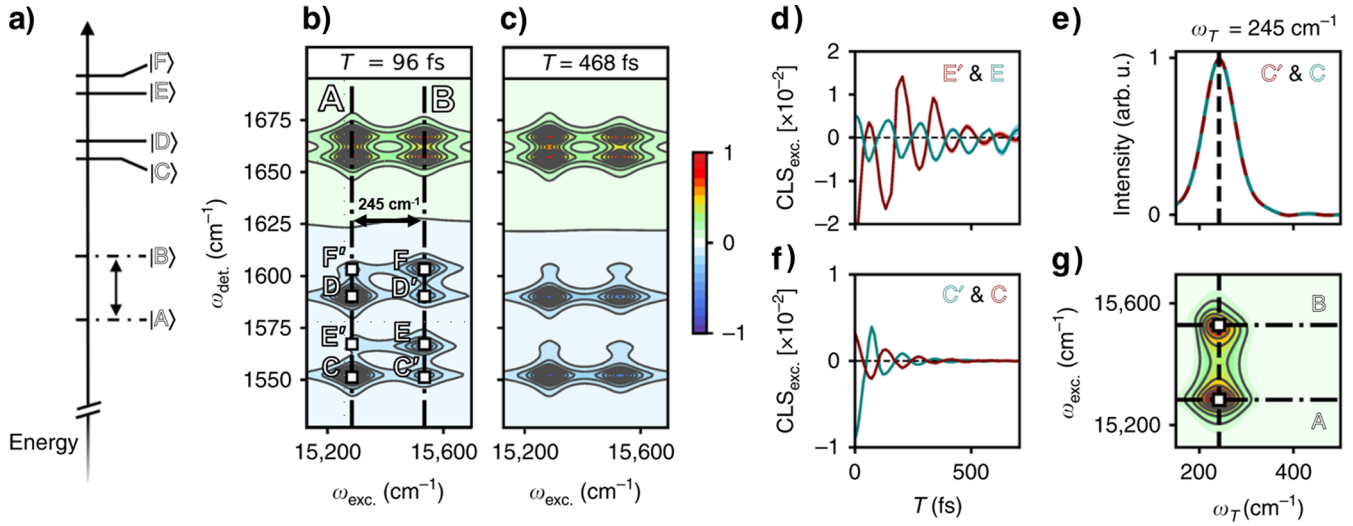

FIG. 16. (a) Energy level diagram for the six excitonic states of the heterodimer model, where the ground state manifold has been omitted for clarity. [(b) and (c)] 2DEV spectra for the model at different waiting times. Positive features indicate ground state bleaches, and negative features indicate excited state absorptions (ESAs). The two ESA quartets are labeled C, E, C′, and E′ and D, F, D′, and F′. The two bands along the excitation axis are marked by the dashed-dotted black lines and labeled by the excitonic state that they originate from (A and B). The $|B\rangle$–$|A\rangle$ energy gap is also labeled. [(d) and (f)] Center line slope dynamics along the excitation axis ($CLS_{exc.}$) of certain features, colored according to the peak labels in the top right corner of each plot. (e) Magnitude of the cross-power spectrum of the CLSs of features C′ and C, where the oscillatory frequency of 245 cm^{-1} is marked by a black dotted line (a peak in the cross-power spectrum indicates a shared frequency). (g) Intensity beat map along the excitation axis of features C′ and C, where the oscillatory frequency of 245 cm^{-1} is marked by a black dotted line and the involved excitation frequencies are labeled and marked by the black dotted-dashed lines. Reproduced with permission from Arsenault *et al.*, Nat. Commun. **11**, 1460 (2020). Copyright 2020 Author(s), licensed under a Creative Commons Attribution 4.0 License.

VII. FUTURE OUTLOOK

In this Perspective, we have illustrated applications of the 2DEVS method to date. We emphasized the improved spectral resolution, the apparently unique information contained in the CLS of the spectral features, and applications to both weakly and strongly coupled molecular complexes. In the following, we explore some of the potential future directions that can be pursued with 2DEVS.

In our discussion of coupled molecular complexes, we introduced models limited to systems containing only a single vibrational DoF per site and did not explicitly distinguish between specific forms of vibronic coupling. However, both the development of multimode models and the explicit treatment of vibronic effects in such models of molecular complexes will be essential to more fully understand experimental 2DEV spectra. For example, it was previously shown by Gaynor and Khalil that the vibronic effects arising from either Franck–Condon or Herzberg–Teller coupling types manifest directly in the positions, line shapes, and amplitudes of the 2DEV spectral features of a monomeric system (limited to one vibrational DoF).[35] In fact, a notable nuclear dependence of the electronic transitions was observed in the models that included non-Condon effects.[35] For coupled systems, a similar, if not more dramatic, effect of differing vibronic mechanisms is expected, which would allow for a direct connection to be made between the observed spectral content and the underlying physical function of the system. This would be a particularly useful measure, for example, as it has been speculated that Herzberg–Teller coupling may be more effective in facilitating ET than the Franck–Condon coupling.[36]

While the bulk of our work has centralized around natural[2,3,19,37] and biomimetic[29,38] photosynthetic systems, this represents only one avenue for the applicability of this technique. For example, Khalil and co-workers elegantly demonstrated how 2DEVS can also be a powerful tool to understand synthetic components utilized for solar conversion.[4,24] Perhaps a fitting future challenge would be the application of 2DEVS to completely understand solar conversion systems with light absorbers, catalysts, and membranes.[39] In particular, 2DEVS should be useful for characterizing the new generation of solid-molecule hybrid systems for solar to fuel conversion based on water splitting. In these systems, the proton motion and CT must be optimized for maximum efficiency,[40–42] and as previously shown, 2DEVS has the unique ability to report on dynamic alterations to the molecular framework (and more) accompanying such processes.

In addition to the possibilities of utilizing 2DEVS to guide and elucidate the function of existing systems, this technique could aid in the development of new, exotic systems where vibronic effects are leveraged. For example, theoretical work has shown that vibronic effects can be exploited in order to drive energy or electron transfer in a way that is thermodynamically uphill.[43] These systems, largely inspired by previous theoretical work suggesting that quantum coherences could be helpful for overcoming local energy traps in the Fenna–Mathews–Olson complex,[44] are termed quantum ratchets. In terms of the role of vibronic effects, resonant vibrational modes were found to play a key role in the maximization of

© Author(s) 2021

unidirectional transport to the acceptor.[43] In particular, the condition of resonance for the transport-promoting vibrational mode was shown to have a remarkable dependence on the Coulombic coupling strength. We speculate that the design and optimization of actual systems that functionalize this phenomenon—thus having the potential to drive ET or CT in an otherwise energetically unfavorable direction—would likely benefit from 2DEVS insights.

Returning to the method, 2DEVS is perhaps most powerful when resolution along both spectral axes is exploited. While significantly improved spectral resolution in systems for which linear, pump–probe, or 2D electronic spectra are unresolved has already been observed, the limit of how large a system can be usefully studied before spectral congestion overwhelms the enhanced capabilities of the method is unknown. Of course, while the specific limitations will be system-dependent, it is interesting to speculate whether ~96 Chls of the photosystem I reaction center core complex would yield any resolvable features in a 2DEV spectrum, for example.[45] Although we did not concentrate on the exploitation of polarization control in 2DEVS, it has been utilized by Lewis and Fleming,[37] Gaynor *et al.*,[24] and Arsenault *et al.*[19] This already provides one approach to further enhance the resolution in congested spectra, as Arsenault *et al.* demonstrated how polarization-associated 2DEV spectra could be generated to separate the evolution of different, overlapping states in highly congested and generally featureless regions of the electronic absorption spectrum of LHCII.[19] A second approach would be to develop two-color 2DEVS, where the two electronic pump pulses are no longer degenerate. In this excitation scheme, population dynamics would be suppressed and only the interaction between specific states of interest would be initially prepared.[46]

While far from mature, 2DEVS has already proven to be a particularly useful method capable of producing a detailed and often nuanced insight into a wide variety of photoactive systems.

ACKNOWLEDGMENTS

This research was supported by the U.S. Department of Energy, Office of Science, Basic Energy Sciences, Chemical Sciences, Geosciences, and Biosciences Division. E.A.A. acknowledges the support of the National Science Foundation Graduate Research Fellowship (Grant No. DGE 1752814). Y.Y. appreciates the support of the Japan Society for the Promotion of Science (JSPS) Postdoctoral Fellowship for Research Abroad. The authors thank Dr. Heinz Frei for insightful comments on the potential applicability of 2DEVS to solar-to-fuel conversion systems.

DATA AVAILABILITY

Data sharing is not applicable to this article as no new data were created or analyzed in this study. Request regarding data should be directed toward the authors of the original works.

REFERENCES

[1] T. A. A. Oliver, N. H. C. Lewis, and G. R. Fleming, Proc. Natl. Acad. Sci. U. S. A. **111**, 10061 (2014).
[2] N. H. C. Lewis, N. L. Gruenke, T. A. A. Oliver, M. Ballottari, R. Bassi, and G. R. Fleming, J. Phys. Chem. Lett. **7**, 4197 (2016).
[3] E. A. Arsenault, Y. Yoneda, M. Iwai, K. K. Niyogi, and G. R. Fleming, Nat. Commun. **11**, 1460 (2020).
[4] J. D. Gaynor, J. Sandwisch, and M. Khalil, Nat. Commun. **10**, 5621 (2019).
[5] P. Hamm, M. Lim, and R. M. Hochstrasser, J. Phys. Chem. B **102**, 6123 (1998).
[6] P. Hamm, M. Lim, W. F. Degrado, and R. M. Hochstrasser, Proc. Natl. Acad. Sci. U. S. A. **96**, 2036 (1999).
[7] O. Golonzka, M. Khalil, N. Demirdöven, and A. Tokmakoff, Phys. Rev. Lett. **86**, 2154 (2001).
[8] J. B. Asbury, T. Steinel, C. Stromberg, K. J. Gaffney, I. R. Piletic, and M. D. Fayer, J. Chem. Phys. **119**, 12981 (2003).
[9] T. Brixner, T. Mančal, I. V. Stiopkin, and G. R. Fleming, J. Chem. Phys. **121**, 4221 (2004).
[10] J. D. Hybl, A. A. Ferro, and D. M. Jonas, J. Chem. Phys. **115**, 6606 (2001).
[11] M. L. Cowan, J. P. Ogilvie, and R. J. D. Miller, Chem. Phys. Lett. **386**, 184 (2004).
[12] M. Cho, Chem. Rev. **108**, 1331 (2008).
[13] P. Hamm and M. Zanni, *Concepts and Methods of 2D Infrared Spectroscopy* (Cambridge University Press, 2011).
[14] M. Cho, *Two-Dimensional Optical Spectroscopy* (CRC Press, 2009).
[15] T. L. Courtney, Z. W. Fox, K. M. Slenkamp, and M. Khalil, J. Chem. Phys. **143**, 154201 (2015).
[16] N. H. C. Lewis, H. Dong, T. A. A. Oliver, and G. R. Fleming, J. Chem. Phys. **142**, 174202 (2015).
[17] M. Cho and G. R. Fleming, J. Phys. Chem. B **124**, 11222 (2020).
[18] H. Dong, N. H. C. Lewis, T. A. A. Oliver, and G. R. Fleming, J. Chem. Phys. **142**, 174201 (2015).
[19] E. A. Arsenault, Y. Yoneda, M. Iwai, K. K. Niyogi, and G. R. Fleming, Nat. Commun. **11**, 6011 (2020).
[20] S. Mukamel, *Principles of Nonlinear Optical Spectroscopy* (Oxford Univeristy Press, 1995).
[21] P. M. Donaldson, H. Strzalka, and P. Hamm, Opt. Express **20**, 12761 (2012).
[22] J. A. Myers, K. L. Lewis, P. F. Tekavec, and J. P. Ogilvie, Opt. Express **16**, 17420 (2008).
[23] Z. Zhang, K. L. Wells, E. W. J. Hyland, and H.-S. Tan, Chem. Phys. Lett. **550**, 156 (2012).
[24] J. D. Gaynor, A. Petrone, X. Li, and M. Khalil, J. Chem. Phys. Lett. **9**, 6289 (2018).
[25] Y. Song, A. Konar, R. Sechrist, V. P. Roy, R. Duan, J. Dziurgot, V. Policht, Y. A. Matutes, K. J. Kubarych, and J. P. Ogilvie, Rev. Sci. Instrum. **90**, 013108 (2019).
[26] J. D. Gaynor, T. L. Courtney, M. Balasubramanian, and M. Khalil, Opt. Lett. **41**, 2895 (2016).
[27] E. C. Wu, Q. Ge, E. A. Arsenault, N. H. C. Lewis, N. L. Gruenke, M. J. Head-Gordon, and G. R. Fleming, Phys. Chem. Chem. Phys. **21**, 14153 (2019).
[28] P. P. Roy, J. Shee, E. A. Arsenault, Y. Yoneda, K. Feuling, M. Head-Gordon, and G. R. Fleming, J. Phys. Chem. Lett. **11**, 4156 (2020).
[29] Y. Yoneda, S. J. Mora, J. Shee, B. L. Wadsworth, E. A. Arsenault, D. Hait, G. Kodis, D. Gust, G. F. Moore, A. L. Moore, M. Head-Gordon, T. A. Moore, and G. R. Fleming, J. Am. Chem. Soc. **143**, 3104 (2021).
[30] R. L. Martin, J. Chem. Phys. **118**, 4775 (2003).
[31] T. Brixner, J. Stenger, H. M. Vaswani, M. Cho, R. E. Blankenship, and G. R. Fleming, Nature **434**, 625 (2005).
[32] N. H. C. Lewis, H. Dong, T. A. A. Oliver, and G. R. Fleming, J. Chem. Phys. **143**, 124203 (2015).
[33] P. Bhattacharyya and G. R. Fleming, J. Phys. Chem. Lett. **10**, 2081 (2019).
[34] Z. Liu, H. Yan, K. Wang, T. Kuang, J. Zhang, L. Gui, X. An, and W. Chang, Nature **428**, 287 (2004).
[35] J. D. Gaynor and M. Khalil, J. Chem. Phys. **147**, 094202 (2017).
[36] H.-D. Zhang, Q. Qiao, R.-X. Xu, and Y. Yan, J. Chem. Phys. **145**, 204109 (2016).
[37] N. H. C. Lewis and G. R. Fleming, J. Phys. Chem. Lett. **7**, 831 (2016).
[38] T. A. A. Oliver and G. R. Fleming, J. Phys. Chem. B **119**, 11428 (2015).
[39] E. Edri, J. K. Cooper, I. D. Sharp, D. M. Guldi, and H. Frei, J. Am. Chem. Soc. **139**, 5458 (2017).
[40] W. J. Jo, G. Katsoukis, and H. Frei, Adv. Funct. Mater. **30**, 1909262 (2020).
[41] D. R. Weinberg, C. J. Gagliardi, J. F. Hull, C. F. Murphy, C. A. Kent, B. C. Westlake, A. Paul, D. H. Ess, D. Granville, and T. J. Meyer, Chem. Rev. **112**, 4016 (2012).

© Author(s) 2021

[42]D. Wang, F. Niu, M. J. Mortelliti, M. V. Sheridan, B. D. Sherman, Y. Zhu, J. R. McBride, J. L. Dempsey, S. Shen, C. J. Dares, F. Li, and T. J. Meyer, Proc. Natl. Acad. Sci. U. S. A. **117**, 12564 (2020).
[43]P. Bhattacharyya and G. R. Fleming, J. Phys. Chem. Lett. **11**, 8337 (2020).
[44]A. Ishizaki and G. R. Fleming, Proc. Natl. Acad. Sci. U. S. A. **106**, 17255 (2009).
[45]P. Jordan, P. Fromme, O. Klukas, H. T. Witt, W. Saenger, and N. Krauß, Nature **411**, 909 (2001).
[46]S. S. Senlik, V. R. Policht, and J. P. Ogilvie, J. Phys. Chem. Lett. **6**, 2413 (2015).

© Author(s) 2021